# Influence of water saturation on the nonlinear elastic mesoscopic response in Earth materials and the implications to the mechanism of nonlinearity

K. E.-A. Van Den Abeele,[1] J. Carmeliet,[2] P. A. Johnson,[3] and B. Zinszner[4]

Received 7 March 2000; revised 13 August 2001; accepted 18 August 2001; published 25 June 2002.

[1] Much is known empirically about the qualitative and quantitative nonlinear response of rocks. Still, the mechanism of nonlinear response in porous media is only speculation. In this work we illustrate evidence from several types of experiments indicating that fluid plays an important role in the nonlinear response. For instance, measurements at low degrees of water saturation indicate that molecular layers of adsorbed moisture as well as condensation fluids significantly influence the linear and nonlinear response at dynamic strain levels due to the activation of internal molecular forces. In rock, we measure a significant increase in the nonlinear response, especially in the saturation range of 1–20%. This is consistent with observed changes in the linear response, but the extent of the variation is larger in the nonlinear measurements, especially in rocks containing small pore systems. These modifications can be attributed to an increased fluid-solid interaction upon wetting causing the material to expand and to soften. Concurrently, the microscopic and mesoscopic hysteretic entities, which give rise to the macroscopically observed nonlinear response, are activated at saturation-dependent opening and closing pressures. As a consequence of the moisture-induced forces, the fraction of active hysteretic units increases with saturation. The fact that the nonlinear response increases with water saturation, especially in the low saturation range, implies that the presence of moisture plays a major role in the nonlinear mechanism or, more precisely, in the activation of that mechanism. *INDEX TERMS:* 5102 Physical Properties of Rocks: Acoustic properties; 3220 Mathematical Geophysics: Nonlinear dynamics; 5139 Physical Properties of Rocks: Transport properties; *KEYWORDS:* material properties, saturation, nonlinearity, nonlinear elasticity, Earth materials, microstructure

## 1. Introduction

[2] On the basis of numerous observations from laboratory studies of rock [*Johnson et al.*, 1996; *Johnson and Rasolofosaon*, 1996] and unconsolidated sedimentary materials [e.g., *Isihara*, 1996; *Hardin and Drnevich*, 1972a, 1972b] and from field studies of nonlinearity in strong ground motion [e.g., *Beresnev and Wen*, 1996; *Field et al.*, 1997], we may conclude that nonlinear response in Earth materials is very large. More recently, it has become clear that damaged solids (plastic, steel, etc.) also display a significantly large nonlinear response that can be qualitatively and quantitatively similar to Earth materials, despite the fact that their nonlinear response is highly localized rather than volumetric, as in Earth materials. It has been suggested that materials exhibiting similar levels of nonlinear behavior, including stress-strain hysteresis, form a class of materials, the nonlinear mesoscopic elasticity class [*Guyer and Johnson*, 1999], which can be described by the Preisach-Mayergosz (PM) space theory of nonlinear elasticity [*Guyer et al.*, 1994, 1995, 1997; *McCall and Guyer*, 1994]. In contrast, materials with atomic elasticity have a small nonlinear response, which is due entirely to their atomic anharmonicity. The latter group of materials is called the classical nonlinear elasticity class which include undamaged individual crystals, many fluids, metals without dislocations, intact plastics, etc. The elastic behavior of these materials can be accurately described by classical Landau theory [e.g., *Hamilton*, 1986; *Naugolnykh and Ostrovsky*, 1998]. On the basis of our experience, it appears that all of the materials in the nonlinear mesoscopic elasticity class have low-aspect ratio features in common (microcracks, macrocracks, grain-to-grain contacts), making them more compressible than atomic elastic materials and leading, in some manner or another, to a larger nonlinear response.

[3] It is well known that at large strain levels, friction between constituents is one of the important mechanisms which contributes to the extreme nonlinearity of porous materials [*Dreyer*, 1972]. However, a lower limit of nonlinear behavior has not been observed [*TenCate and Shankland*, 1998], even at strains of $10^{-9}$ and displacements approaching atomic dimension, where it is unlikely that mechanical frictional effects take place.

[1]Interdisciplinary Research Center, Faculty of Science, Catholic University Leuven Campus Kortrijk, Kortrijk, Belgium.
[2]Laboratory of Building Physics, Department of Civil Engineering, Catholic University Leuven, Leuven, Belgium.
[3]Earth and Environmental Sciences Division, Los Alamos National Laboratory, Los Alamos, New Mexico, USA.
[4]Institut Français du Pétrole, Rueil-Malmaison, France.


0148-0227/02/2001JB000368$09.00

[4] Low-aspect ratio features and microinhomogeneous imperfections can be conduits for moisture. Fluids can change the linear behavior of mesoscopic materials in well-known, dramatic manners. Especially in the low saturation range where molecular adsorption and capillary condensation (formation of menisci) occurs, a significant decrease of elastic moduli is observed in porous media [e.g., *Bourbié et al.*, 1986]. It is not unreasonable to hypothesize that a similar effect may persist and govern the nonlinearity of wetted pore surfaces and contacts in porous materials. Indeed, it is well-known in atomic force microscopy that the presence of moisture can produce nonlinear and hysteretic effects between the probe and a wetted surface [*Binggeli and Mate*, 1995; *Capella and Dietler*, 1999].

[5] Thus we have evidence suggesting that (1) nonlinearity is related to microscopic and mesoscopic structural features; (2) linear elastic behavior in mesoscopic porous solids can be greatly influenced by the presence of fluids; (3) nonlinear and hysteretic surface forces associated with wetting are widely observed; and (4) a limit to the nonlinear response is not observed, even at the smallest strains measured ($\sim 10^{-9}$) where mechanical frictional effects are absent. Taken as a whole, these observations imply that the role of fluids must be important in the nonlinear behavior of microinhomogeneous materials.

[6] The focus of the work presented here is to investigate in greater detail the influence of fluids on the linear and nonlinear response of rock and to draw conclusions from these observations. First, we will illustrate linear and nonlinear dynamic properties measured in the range of 0.1% to +99% water saturation and at ambient pressure conditions for two different rock types (two sandstones and one limestone). We will also show evidence of moisture influence from linear dynamic tests at increasing confining pressure taken at water saturation levels near zero and near 100%. Second, we focus on a combined theoretical and experimental prediction of the microstuctural fluid-solid interaction forces that are involved in the saturation process. To this extent, we first define the dominant moisture induced forces at the microscopic level and the equivalent macroscopic force assuming thermodynamical and mechanical equilibrium conditions. Then we measure the saturation as function of the capillary pressure, which is the chemical pressure difference between the phases of liquid water and mixed water vapor with dry air at the meniscus. In the third stage, we express the linear and nonlinear measurements in terms of the chemical pressure. This allows identification of the range of microstresses where the moisture induced activation of the linear and nonlinear properties is most pronounced. That is, are capillary forces more important than molecular adsorption forces, for instance. As a final topic in the discussion, we connect our observations of the moisture dependent elastic response in rocks with the phenomenological PM space model of *McCall and Guyer* [1994] for the description of nonlinear quasi-static and dynamic behavior of microinhomogeneous hysteretic media.

## 2. Linear and Nonlinear Properties Versus Saturation

[7] In this section, we report on the dynamic experiments and observations at various saturation levels.

### 2.1. Experiments

[8] Two types of dynamics experiments are performed: (1) linear and nonlinear resonance experiments on rock samples at various levels of saturation under ambient pressure conditions and (2) linear dynamic measurements at external confining pressures. We used the resonance method for extracting the dynamic linear and nonlinear behavior of three rock samples. The nonlinearity is quantified by studying the resonance frequency shift of the fundamental mode as a function of drive level [e.g., *Johnson et al.*, 1996; *Zinszner et al.*, 1997; *TenCate and Shankland*, 1998; *Van Den Abeele et al.*, 2000b]. The second group of measurements were made in a pressure vessel at two saturation states (dry and fully saturated), using the resonance method as well [*Zinszner et al.*, 1997].

#### 2.1.1. Rock samples

[9] Two different rock types with very different internal structure were studied: Lavoux limestone and Berea and Meule sandstone. The limestone is a pelletoidal rock, composed of 99% calcium carbonate (calcite). Meule and Berea sandstone are composed of quartz grains and contain a considerable amount of clay and other secondary mineralization. The bonding material is primarily silica. Physical properties and dimensions of these rocks are shown in Table 1.

#### 2.1.2. Dynamic resonance measurements

[10] The basic elements of the experimental configuration for obtaining frequency versus acceleration measurements are shown in Figure 1. A frequency sweep interval is chosen to encompass frequencies well above and well below the fundamental resonance mode of the sample. For cylindrical samples (Lavoux and Meule) we studied the lowest-order longitudinal mode. The Berea sandstone samples were cut into beams (elongated rectangular parallelepipid), and the study was conducted on the lowest-order bending mode. The samples are excited either by an electromagnetic (coil/magnet), piezoelectric, or shaker-type source affixed to the sample (longitudinal mode study) or by a noncontact speaker coupled through air (flexural mode study). At each frequency of excitation the response signal is detected by a calibrated accelerometer and analyzed to obtain amplitude and phase of the input frequency wave. The input is stepped through the frequency band of interest, and the acceleration amplitude (output) is recorded as function of the drive frequency. Typically, 5–20 stepped sine experiments are conducted at successively increasing drive voltages over the same frequency interval in order to monitor resonant peak shift and harmonic generation for extraction of the nonlinear response. Time series signals are captured as well for Fourier analysis.

[11] Measurements were taken at numerous water saturation levels between ~0.1 and 99%. For Lavoux and Meule the samples were 100% saturated after oven drying and then saturating under vacuum. Measurements were made as the rock slowly dried under room conditions, ensuring a uniform moisture distribution over the specimen. For Berea the measurements started at the capillary water saturation level (free imbibition). Densities were derived from the dry and wet weights [*Bourbie et al.*, 1986].

#### 2.1.3. Pressure vessel measurements

[12] The resonant bar pressure vessel is described by *Lucet et al.* [1991] and *Zinszner et al.* [1997]. In order to

**Table 1.** Physical Rock Properties, Dimensions, and Measurement Parameters

| Rock | Rock Type | Density, kg/m$^3$ | Porosity, % | Young's Modulus, MPa | Compressive Strength, MPa | Geometry | Frequency Range $f$ in Dynamic Resonance |
|---|---|---|---|---|---|---|---|
| Lavoux limestone | pelletoidal limestone 99% calcite | 2049 | 24.2 | 17 | 25 | cylindrical length: 115 cm; diameter: 5.0 cm | 1.1–1.25 kHz |
| Meule sandstone | fine-grained, argillaceous micaceous sandstone 74% quartz 21% feldspar 2% smectite 2% mica/illite 1% kaolinite | 2077 | 21.8 | 8.5 | 35 | cylindrical length: 107.6 cm diameter: 9.0 cm | 550–950 Hz |
| Berea sandstone | fine-grained sandstone 85% quartz 8% feldspar 5% kaolinite 1% smectite 1% mica/illite | 2186 | 18.6 | 8.2 | 32 | beam length: 25.5 cm width: 2.6 cm Thickness: 0.95 cm | 200–320 Hz |

perform measurements under effective pressure, the bar is jacketed and sealed. (Effective pressure is the confining pressure minus the pore pressure.) The pore pressure is assumed to be in equilibrium with the atmosphere. The bar is supported in the center to avoid clamping effects on the fundamental resonant mode. A source and a detector are affixed to the sample, similar to the experiments at ambient conditions. The small mass loading effects [*Lucet et al.*, 1991] are not accounted for because we are studying relative, not absolute, changes. Low excitation (linear) resonance measurements are performed inside the vessel in the same manner as described above.

[13] The linear properties (elastic modulus and attenuation) of Lavoux and Meule samples were studied under different effective pressures at two states of fluid saturation. First, measurements were made in the dry state after oven drying at 70°C. Measurements were also made at 100% tap water saturation. In all of the above experiments, comparative studies were conducted using atomic elastic standards (aluminum, PVC, Plexiglas, Pyrex glass, etc.) to be certain that the apparatus was not contributing to the nonlinearity.

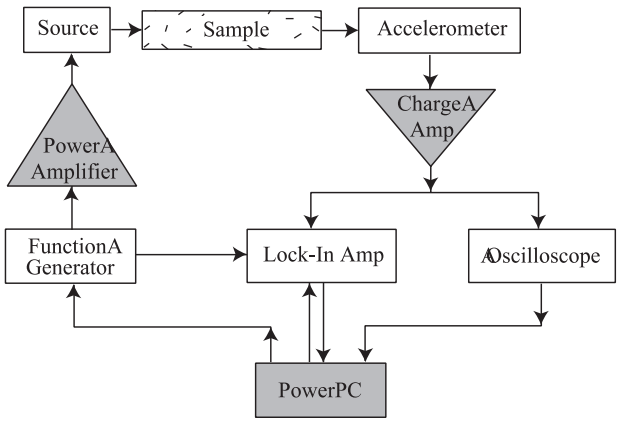


**Figure 1.** Basic elements of a resonant bar experiment.

### 2.1.4. Dynamic characteristics

[14] The linear quality factor $Q$ (inverse attenuation) is obtained in the standard manner from the half width at half maximum of the resonance peak at low excitation. The linear Young's modulus ($E$) is calculated from the resonance frequency peak and the measured density ($\rho$) at each saturation level:

$$\text{For cylindrical samples} \qquad E = (2Lf_0)^2\rho \tag{1a}$$

$$\text{For beams} \qquad E = \left[\frac{8\sqrt{12}}{\pi\ d}\left(\frac{L}{3.0122}\right)f_0\right]^2\rho, \tag{1b}$$

where $L$ is sample length, $d$ is its thickness (for beams), and $f_0$ is the low excitation resonance frequency. The typical frequency range for the dynamic resonance experiments and the correspondingly calculated Young's moduli for the three different rocks are listed in Table 1.

[15] The nonlinearity property is derived from the change in resonance frequency with calculated strain amplitude ($\varepsilon$), normalized to the linear resonance frequency, i.e., $(f_0 - f(\varepsilon))/f_0$ or $\Delta f(\varepsilon)/f_0$ [see, e.g., *Van Den Abeele et al.*, 2000b]. In short, the change in frequency represents the softening of the modulus induced by wave excitation, which is one possible measure of the nonlinear response. Strain amplitude ($\varepsilon$) is calculated from the measured acceleration amplitude ($A$) in the following manner:

$$\text{For cylindrical samples} \qquad \varepsilon = \frac{A}{4\pi L f^2} \tag{2a}$$

$$\text{For beams} \qquad \varepsilon = \frac{0.219}{f^2}\frac{\pi}{8}\frac{d}{\sqrt{12}}\left(\frac{3.0112}{L}\right)^2 A. \tag{2b}$$

In rocks we found a ubiquitous linear decrease of the resonance frequency as function of the strain amplitude at

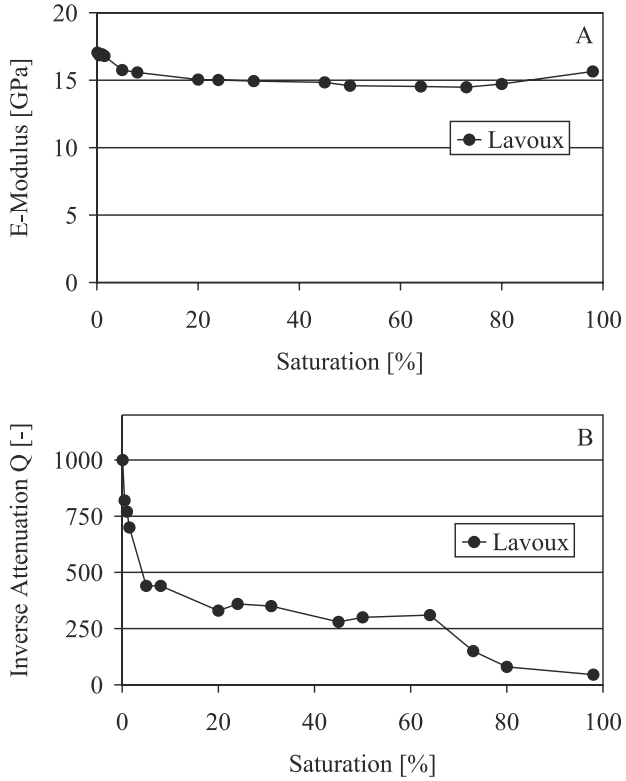


**Figure 2.** (a) Young's modulus $E$ and (b) inverse attenuation $Q$ as function of saturation for Lavoux limestone.

all saturation levels. The proportionality coefficient "$\alpha$" relating the relative frequency shift to the strain amplitude is used to quantify the nonlinearity:

$$\frac{\Delta f(\varepsilon)}{f_0} = \frac{f_0 - f(\varepsilon)}{f_0} = \alpha\varepsilon. \tag{3}$$

It is well known that the proportionality coefficient $\alpha$ is a measure of the dynamic stress-strain hysteresis [*Guyer et al.*, 1994, 1995; *McCall and Guyer*, 1994; *Van Den Abeele et al.*, 1997, 2000a, 2000b]. It is important to note that these findings are essentially different from a classical nonlinear oscillator, such as the Duffing type oscillator [*Stoker*, 1950]. A classical treatment of nonlinear oscillations, using a power law expansion of the constitutive equation, always predicts a quadratic decrease of the resonance frequency with increasing drive voltage. Several experimental observations of nonlinearity in rocks, both from static and dynamic tests, clearly argue that the nature of their nonlinearity is merely hysteretic, and not "classical atomic" [*Guyer et al.*, 1994; *Johnson et al.*, 1996; *Johnson and Rasolofosaon*, 1996; *Van Den Abeele et al.*, 1997, 2000a, 2000b]. A classical nonlinear approach is simply not adequate to describe the observed phenomena. Our measurements confirm that the (purely) hysteretic nature of rocks is a reasonable assumption. In the following, we discuss the evolution of the inverse attenuation ($Q$), the linear modulus ($E$) and the dynamic hysteresis coefficient ($\alpha$) as function of saturation ($S$) for Lavoux, Meule, and Berea.

## 2.2. Observations

### 2.2.1. Limestone

[16] The linear modulus $E$ and inverse attenuation $Q$ for Lavoux limestone are shown in Figure 2 as function of the saturation level. The observed changes are typical for the moisture dependence of the linear dynamic properties of rocks [e.g., *Bourbié et al.*, 1986]. We see a moderate change in the linear modulus of $\sim$15% from 0.1% to 70% water saturation. Over the same saturation interval, the quality factor $Q$ decreases by $\sim$95%.

[17] In Figure 3 the nonlinear response is illustrated as function of saturation: Figure 3a shows a subset of the actual measured values of the relative frequency shift as function of the inferred strain at different saturation levels. Notice the universal proportionality of the frequency shift with respect to the measured strain (equation (3)). The evolution of the nonlinearity coefficient $\alpha$ as function of saturation is shown in Figure 3b. There is a clear progression from less to more nonlinear as saturation increases from 0.1% to 31%, changing by one order of magnitude. Above 30%, the nonlinear response levels off. Note that the change in linear velocity with saturation, as observed in Figure 2, is eliminated by normalizing to $f_0$ (as in equation (3)).

### 2.2.2. Sandstone

[18] The linear Young's modulus as a function of saturation is shown in Figure 4 for Meule and Berea (the $Q$ response was also measured but is not shown here).

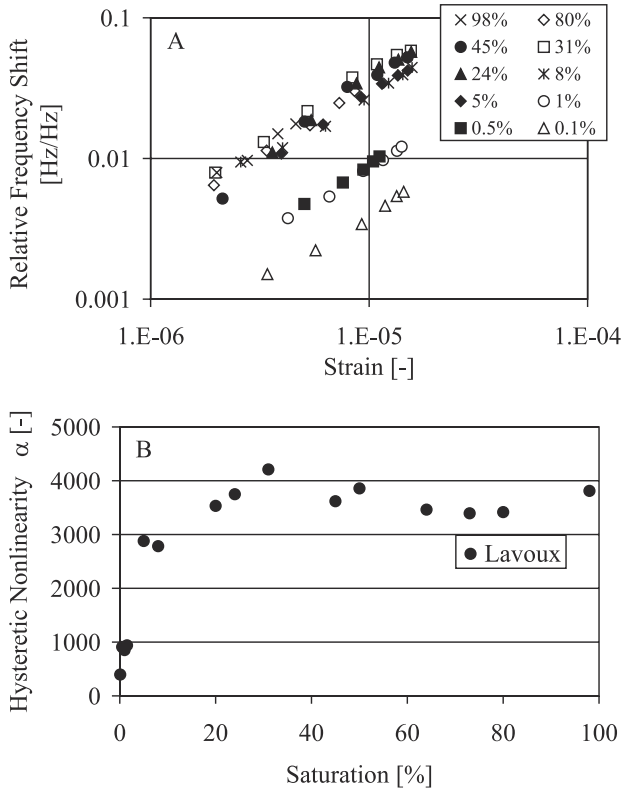


**Figure 3.** Changes in nonlinear response as function of saturation for Lavoux limestone. (a) Relative resonance Frequency shift versus inferred strain for different saturation levels. (b) inferred hysteretic nonlinearity coefficient $\alpha$ as function of saturation.

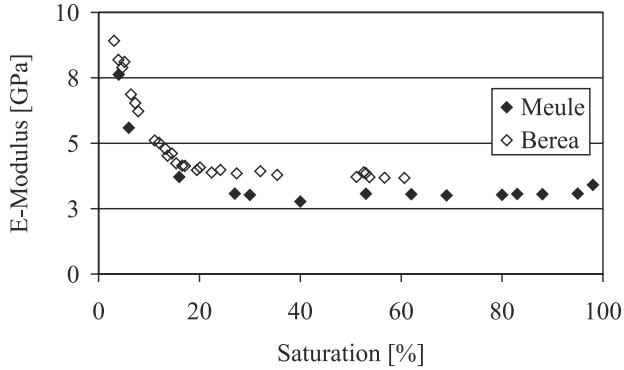


**Figure 4.** Young's modulus $E$ as function of saturation for Meule and Berea sandstone.

Between 0 and 20%, we see a much larger change in linear modulus with saturation than in the limestone. The modulus changes very little beyond ~20% saturation. These are common differences in observations between sandstone and limestone and are generally attributed to the distinct type of pore space geometry [see, e.g., *Lucet et al.*, 1991; *Bourbié et al.*, 1986].

[19] Figure 5 shows the nonlinear response of the two sandstones as a function of saturation, quantified in terms of the above defined hysteretic nonlinearity coefficient. We observe once again an initial sharp increase in the nonlinear response with water saturation. The maximum nonlinearity is observed in the range of 5–10% water saturation, after which the nonlinear response decreases gradually with saturation.

### 2.2.3. Pressure vessel results

[20] In a qualitative manner, the pressure vessel results for dry conditions and at full saturation, shown in Figure 6, support the above observations. Figure 6a illustrates that the linear velocity (or, equivalently, the modulus) for Lavoux under dry conditions changes very little as function of the externally applied effective pressure, whereas the velocity and modulus become more pressure-dependent and much more hysteretic at full saturation. The measurements made on Meule sandstone (Figure 6b) show a similar behavior. In Figure 7 we plot the relative change in linear, longitudinal velocity at 100% saturation ($S = 100$) versus the relative change in longitudinal velocity in oven-dry conditions ($S = 0$) measured at the same pressure levels: i.e., $\delta V_{100}(P)$ is plotted versus $\delta V_0(P)$, where $\delta V_i(P) = [V_i(P) - V_i(0)]/V_i(0)$ for $i = 0, 100$. For Meule (Figure 7b) the obtained relationship reveals that the relative change in velocity (modulus) for fully saturated samples is larger by a constant factor 2 over the entire pressure range in comparison with a dry sample. For Lavoux (Figure 7a) we obtained a steeper increase at low pressures (factor 8) than at high pressures (factor 4). The increases by a factor 2 (for Meule) and 8 (for Lavoux) are in quantitative agreement with the increase of the nonlinearity coefficients at these saturation levels observed in dynamic resonance experiments at ambient pressure conditions. Indeed, in Figure 5 (Meule) we note an increase in nonlinearity from 2500 ($\alpha_{dry}$) to 5000 ($\alpha_{sat}$), and in Figure 3b (Lavoux) $\alpha$ changes from 500 to 4000. One could conclude from these observations that moisture plays a similar physical role in the behavior of both the linear and nonlinear elasticity. However, one has to interpret this statement with great care. The agreement does not necessarily imply for instance that the changes originate from a common physical effect. On the basis of the PM space description of elasticity in rocks [*Guyer et al.*, 1994, 1995; *McCall and Guyer*, 1994], we know that the change in linear velocity refers to a change of the reversible nonlinear elastic units that build up the material. The moisture dependence of $\alpha$ refers to the change of the hysteretic elastic units upon changes in saturation. We expect the same tendencies, but surprisingly,

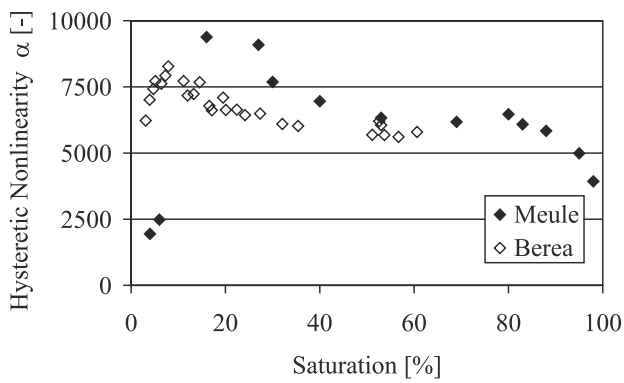


**Figure 5.** Inferred hysteretic nonlinearity coefficient $\alpha$ as function of saturation for Meule and Berea sandstone.

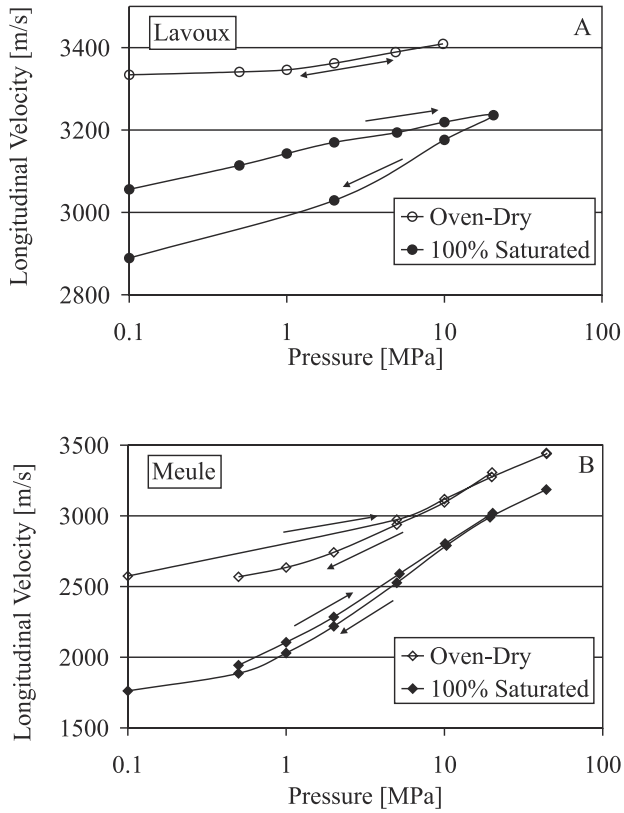


**Figure 6.** Pressure vessel velocity measurements as function of the confining pressure for oven-dry and 100% water-saturated samples of (a) Lavoux and (b) Meule [from *Zinszner et al.*, 1997].

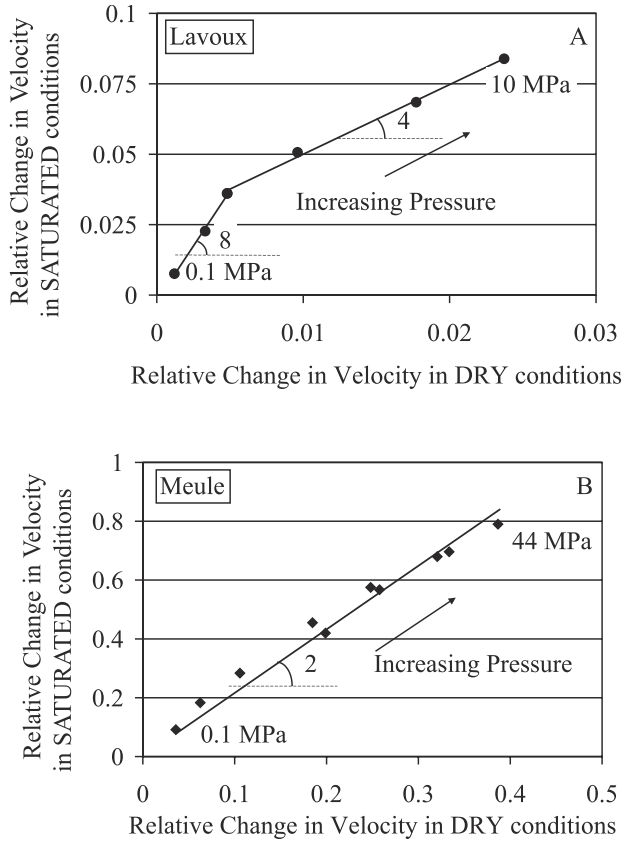


**Figure 7.** Relative change in longitudinal velocity under 100% saturation conditions versus the relative change in longitudinal velocity under oven-dry conditions measured at the same pressure levels for (a) Lavoux and (b) Meule. Owing to the extreme hysteresis observed in the saturated Lavoux data, we used the mean of the interpolated velocities at each pressure level. For Lavoux a ratio of 8 is found at low pressures, followed by a more moderate proportionality at high pressures (factor 4). For Meule the analysis reveals that the relative change in longitudinal velocity for $S = 100$ is increasing on average twice as fast over the entire pressure range compared to the relative change in longitudinal velocity in oven-dry conditions.

we also observe the same relative ratio's (which is something that has to be confirmed by further analysis).

[21] In the above experiments we have illustrated that the nonlinear response of rock samples changes significantly with saturation, in particular, between 0% and 10–25% water saturation. At the same time, there is a notable change in the linear properties such as dissipation and wave speed. We also alluded to a possible concordance as to the influence of water saturation on the mechanism of nonlinear and linear elastic behavior. It is clear that this influence is to be found on the microstructural level. In section 3 we will express and analyze the above observations in the context of the internal forces induced by the presence of moisture.

## 3. Moisture-Induced Microforces

[22] Rocks are hydophilic materials and contain a huge specific (internal) surface area due to pore space. Consequently, they may exhibit intense fluid-matrix interactions which can be attributed to molecular and surface forces. The induced forces are known to be extremely sensitive to the level of fluid saturation [e.g., *Carmeliet et al.*, 1999]. Solid fluid pressures include molecular adsorption forces along pore walls, capillary pressures in capillary pores, and interlayer fluid pressures due to the presence of interlayer hydrate water in nanopores. For convention, we assign positive pressures to an expansive loading and negative pressures to contraction.

[23] In the following we illustrate and discuss the relation between the linear and nonlinear elastic phenomena and the moisture-induced forces which are present as function of the saturation. First, we identify the various moisture-induced forces at the microscopic level. Next, we interpret the global influence of the microscopic forces on a macroscopic level and establish the link between the equivalent macroscopic force and the level of saturation. Using this information base, we relate the effective influence of the microscopic forces on a macroscopic level to the observed moisture dependence of the linear and nonlinear elastic properties of the two rock types.

### 3.1. Moisture-Induced Forces at the Microscopic Scale

[24] At very low saturation levels the adsorption process is governed by the interaction of repulsive and attractive forces between the water molecules and the molecules or ions of the solid. Water adsorption is a consequence of the larger molecular attraction forces of water molecules to the solid than the binding forces of gas molecules to the solid [*Israelachvili*, 1985]. Upon balancing the forces, the layers of adsorbed water on the pore walls exposed to water vapor are subjected to a microscopic spreading pressure, which reduces the surface free energy of the solid. This spreading pressure decreases with increasing distance from the solid wall.

[25] At higher levels of saturation, capillary condensation takes place. Capillary condensation commences when the molecular adsorbed water layers in the finest pores abruptly alter to a more stable arrangement due to surface tension. As a result, a meniscus is formed between the liquid water ($l$) and the gas ($g$) phase (Figure 8). As one may expect, this sudden transition does not occur uniformly over the entire sample. It is highly dependent on the range of pore dimensions inherent to rocks. Under certain restricted conditions (isothermal, no salts, etc.) the chemical potential governing the capillary condensation process can be expressed in terms of the microscopic capillary pressure, $\pi_c$, which is defined as the difference between the pressure in gaseous and liquid phases across the meniscus:

$$\pi_c = \pi_g - \pi_l. \tag{4}$$

Kelvin's law relates the microscopic capillary pressure $\pi_c$ to the pore relative humidity (RH) above the meniscus and states that isothermal thermodynamic equilibrium at the meniscus occurs when

$$\ln(\mathrm{RH}) = -\frac{\pi_c}{\rho_l R_v T} \tag{5}$$

with RH the relative humidity, $\pi_c$ the capillary pressure, $\rho_l$ the density of liquid water (1000 kg/m$^3$), $R_v$ the universal

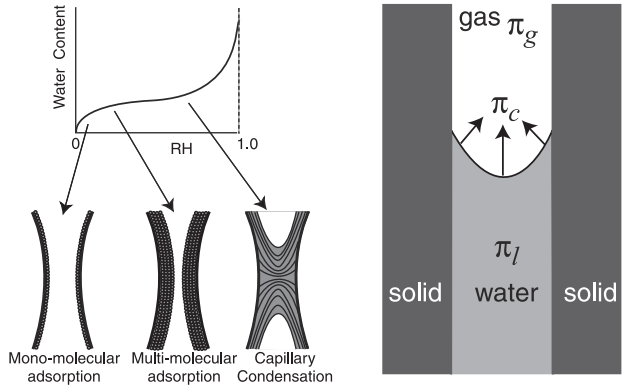


**Figure 8.** Sorption processes: adsorption and capillary condensation.

gas constant for water vapor (462 J/kg K), and $T$ the room temperature (293 K).

[26] Since the microscopic capillary pressure $\pi_c$ (in absence of external loads) is always positive, it exerts an tensile loading on the pore water leading to a microscopic contraction pressure $\pi_c^R$ as a reaction force in the solid (Figure 9a). According to Kelvin's law (equation (5)) the microscopic capillary pressure is a decreasing function of the relative humidity (e.g., at RH = 0.4 (20°C), $\pi_c$ = 124 MPa, and at RH = 0.9, $\pi_c$ = 14 MPa).

[27] In a very fine pore system it is possible that the full thickness of the adsorption layers cannot develop for a given RH and that water adsorption is hindered. A microscopic swelling pressure, $\pi_s$, arises as a result of repulsion forces between water molecules, keeping the pore walls at a certain distance [*Powers*, 1965; *Wittmann*, 1974; *Bazant*, 1970]. Typical examples of such fine pore structures can be found in media which are rich in clays and calcium-silicate-hydrate (CSH) particles, composed of laminar sheets with interlayer adsorbed water. The repulsive forces at the solid surfaces drive the laminar sheets apart and the cohesive forces between the solid walls decrease. As a result, the adsorbed water experiences a microscopic compressive force. These microcompressive liquid forces are balanced by expansive microforces $\pi_S^R$ in the solid (Figure 9b). Bazant shows that the swelling pressure can be extremely high. For example, in a pore that is only two water molecules thick, $\pi_S^R$ = 174 MPa at RH ≈ 1. Although no thermodynamical proof exists, $\pi_S^R$ is generally considered to be dependent on the relative humidity according to a Kelvin-type law [*Bazant et al.*, 1997].

[28] In summary, the microscopic capillary pressure (tensile microforce on the fluid, always positive) decreases with increasing degree of saturation, which results in a decrease of the reactive microscopic contraction of the solid (or an increase of expansion). The microscopic swelling pressure (always negative: compressive microforce on the fluid) increases in absolute value with increasing degree of saturation, giving rise to increasing microscopic expansive reaction forces in the solid. When microscopic capillary pressures are dominant, the solid material will sustain a microscopic contraction. When swelling pressures prevail, the material matrix will experience expansive microstresses. Without making further assumptions about the real dependence of the swelling pressure on RH, we may assume that the

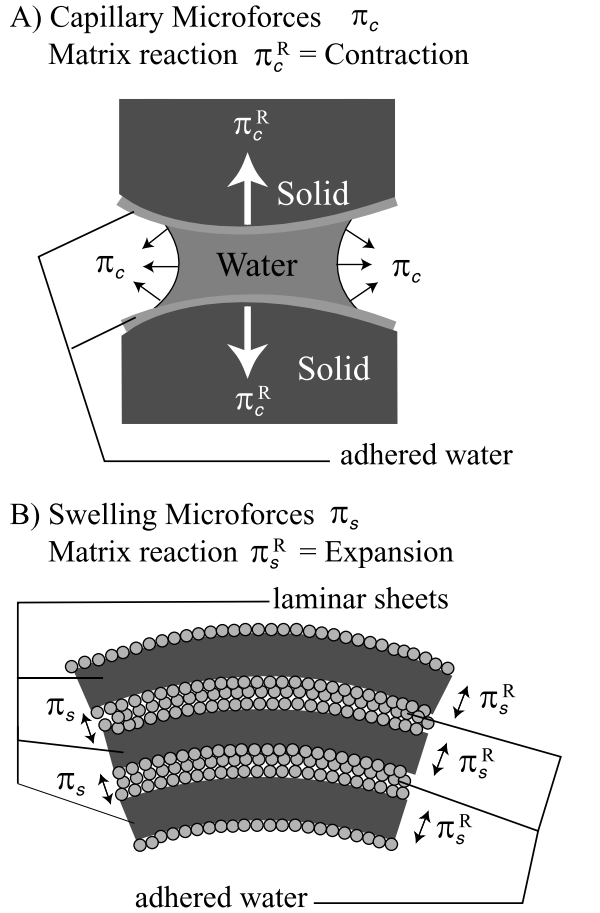


**Figure 9.** Moisture-induced microforces: (a) capillary and (b) swelling pressure which induce competing microscopic matrix reaction.

net microscopic reaction pressure effect results in either contraction or expansion of the solid. As saturation increases, the reactive loading of the solid will evolve from strong contraction to less contraction or even expansion and from low expansive loading toward a more extreme expansion of the solid (Figure 10).

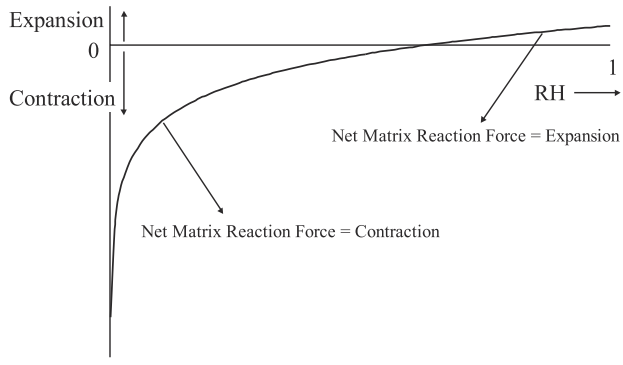


**Figure 10.** Solid matrix reaction due to microscopic capillary and swelling pressures. If microscopic swelling pressure is important (e.g., in materials with clays and CSH particles), the net force can lead to an expansive matrix reaction near RH = 1. This effect is highly exaggerated in this figure for illustrative purposes.

### 3.2. Equivalent Macroscopic Forces and State Relation

[29] We now assume that all pore water in the microstructure is locally in thermodynamic equilibrium. Therefore changes in microscopic capillary pressure will almost instantly result in changes of microscopic swelling pressure and interlayer water pressure. The net result of all moisture induced microstresses on the liquid can then be expressed at the macroscale by one macroscopic liquid pressure $p_l$. This macroscopic liquid pressure can be seen as the average result of all the microscopic pressures acting at the pore scale. Assuming the gaseous phase in thermodynamic equilibrium with the outside ($p_g$ at constant atmospheric pressure), the macroscopic liquid pressure $p_l$ can be replaced by the macroscopic capillary pressure $p_c$ ($p_c = p_g - p_l$), which is commonly used in fluid transport modeling [*Bear and Bachmat*, 1991]. In this context, the macroscopic capillary pressure can be considered to be representative of the combined effects of all complex microscopic fluid-solid interaction forces.

[30] The linear and nonlinear acoustic measurements we discussed in section 2 of this paper were expressed as a function of the degree of saturation $S$. The relation between the degree of saturation and the macroscopic capillary pressure $p_c$ is referred to as the capillary pressure curve: $S(p_c)$. In order to obtain the capillary pressure (or water retention) curves we performed mercury intrusion experiments on all three rocks in addition to measurements of adsorption isotherms (for details on mercury porosimetry, see *Orr* [1969] and *Van Brakel et al.* [1981]). The experimentally obtained state relation can be fit in an analytical form by a sum of power functions [*van Genuchten*, 1980; *Durner*, 1994; *Carmeliet et al.*, 1999]

$$w(p_c) = w_{\mathrm{sat}} \sum_{i=1}^{k} l_i \left[1 + (c_i p_c)^{n_i}\right]^{\left(1-\frac{1}{n_i}\right)}, \qquad (6)$$

where $k$ is the number of power functions and $l_i$ are the weighting factors ($0 < l_i \leq 1$, $\Sigma l_i = 1$). The fully saturated moisture content $w_{\mathrm{sat}}$ is defined as the moisture content upon complete filling of the open porosity with water. This value can be determined in a separate vacuum saturation experiment. The analytic approximations of the water retention curves obtained by fitting the measurement data to equation (6) for the three different rocks (Berea, Meule, and Lavoux, normalized to the respective $w_{\mathrm{sat}}$ values) are illustrated in Figure 11. The fitting parameters are summarized in Table 2. There is a clear difference between Lavoux limestone and the two sandstones. At saturation levels of 25% and above, the limestone is subjected to much higher internal forces compared to the two sandstones.

**Table 2.** Fitting Parameters of the Water Retention Curves Used in Equation (6) for Lavoux Limestone, Meule Sandstone, and Berea Sandstone[a]

| Rock | $w_{\mathrm{sat}}$, kg/m$^3$ | Index | $l$ | $c$ | $n$ |
|---|---|---|---|---|---|
| Lavoux | 251 | 1 | 0.3149 | 1.66E-06 | 3.5343 |
| | | 2 | 0.5114 | 5.82E-06 | 1.8470 |
| | | 3 | 0.1737 | 8.81E-06 | 8.4693 |
| Meule | 219 | 1 | 0.0627 | 1.18E-07 | 1.7591 |
| | | 2 | 0.4583 | 3.02E-05 | 1.4392 |
| | | 3 | 0.4790 | 4.03E-05 | 8.3748 |
| Berea | 186 | 1 | 0.2868 | 6.07E-06 | 1.5920 |
| | | 2 | 0.5080 | 4.59E-05 | 3.5004 |
| | | 3 | 0.2053 | 5.45E-05 | 9.8465 |

[a]In all cases, $k = 3$. Read 1.66E-06 as $1.66 \times 10^{-6}$.

### 3.3. Implications of Moisture on Dynamic Properties

#### 3.3.1. Range of moisture influenced dynamics

[31] Now that we have quantified the state relation $S(p_c)$, we can express the measured linear and nonlinear parameters as a function of the equivalent macroscopic capillary pressure. Figure 12 shows that the primary changes in the

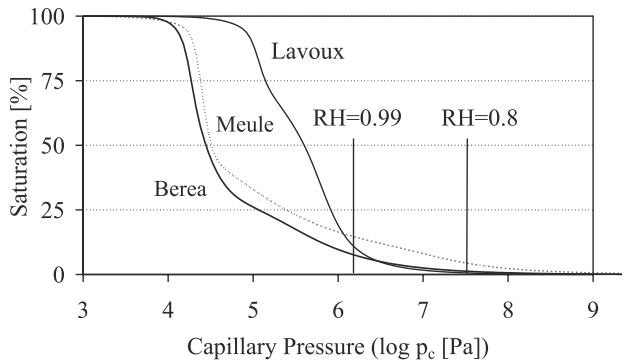


**Figure 11.** Capillary pressure (water retention) curves of Lavoux limestone and Meule and Berea Sandstone, measured by mercury intrusion.

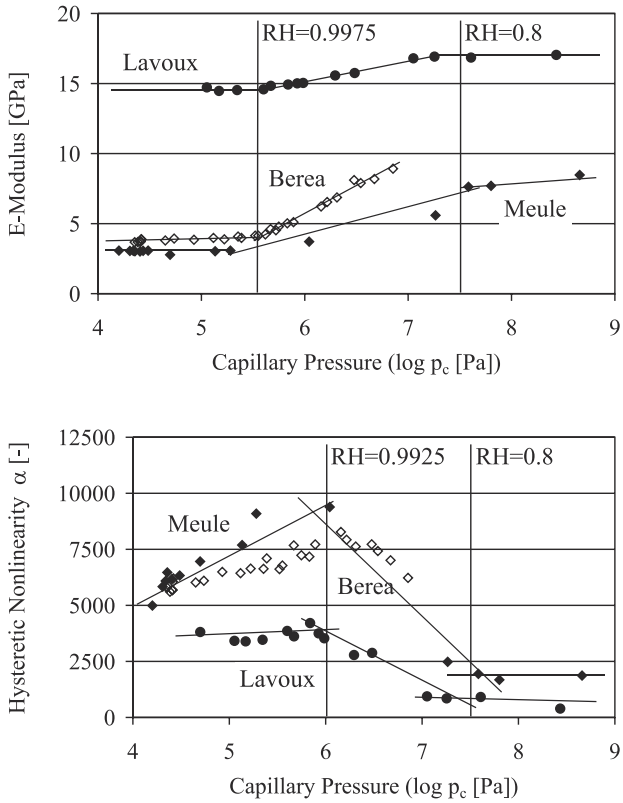


**Figure 12.** Linear and nonlinear parameters as function of the macroscopic capillary pressure for Lavoux, Meule, and Berea. The straight lines are purely guides for the eye.

linear and nonlinear parameters are restricted to small ranges of capillary pressures. (The straight lines are purely guides for the eye.) In terms of relative humidity, the changes occur in range 0.8–0.9975 RH, where the microscopic capillary pressures and swelling pressures prevail, and the microscopic adsorption forces are of less importance. It is remarkable that the nonlinear coefficients for Berea and Meule decrease again at lower capillary pressures. The values of relative humidity noted on the figures correspond to the relative humidity which can be calculated starting from the saturation level $S$ of the sample (determined in the experiments by weight), then relating $S$ to the macroscopic capillary pressure through the state relation $S(p_c)$, and finally using the macroscopic equivalent of Kelvin's law (5) to obtain RH.

### 3.3.2. Macroscopic implications

[32] The perception of moisture-induced microforces has some interesting implications, which are in agreement with the observations.

1. The decrease of microscopic contraction of the matrix with the degree of saturation obviously results in a swelling and a reduction of the stiffness property of the material.

2. At the same time, the mobility of the constituent particles increases, and likewise the number of nonlinear and/or hysteretic microinhomogeneities (grain-to-grain boundaries, asperities, microcracks, etc., also termed nonclassical units, NCU, see later) and their ability to change states (contact-no contact; open-close; pin-unpin) increases with the degree of saturation. Therefore an increase of nonlinear elastic effects is expected.

3. At complete saturation (98% and up) the apparent stiffness of the wet material can increase again due to the stiffening effect of the water, which acts as a one phase solid material sustaining part of the external load.

4. From XRD analysis (Table 1) and thin section analysis (not illustrated) we know that both Meule and Berea sandstone have at least some percentage of clays and CSH particles and must be sensitive to swelling pressures. The effect of the swelling pressure can lead to an extreme expansive microloading, which may inactivate microinhomogeneities and exclude them from contributing to the macroscopic nonlinear behavior of the material, resulting in a reduction of the nonlinearity parameter. It is expected that Lavoux limestone is less sensitive because of its nearly pure composition of calcite. In this case, a saturation of the macroscopically observed nonlinearity is expected.

5. Finally, the increasing swelling pressure with saturation may explain in part the observe reduction of the tensile strength of a material at higher degrees of saturation (an observation that is not shown here but is well known in literature [e.g., *Hiller*, 1964]).

### 3.3.3. Implications for PM space modeling

[33] As a final remark, we link our observations to the current state-of-the-art model that is used to describe static and dynamic nonlinear behavior in rock-type materials. On the basis of the work of F. Preisach and I. Mayergoyz, R. A. Guyer and K. R. McCall have developed a phenomenological model to describe the quasi-static stress-strain relation in rocks [*Guyer et al.*, 1994, 1995, 1997; *McCall and Guyer*, 1994]. In this model, called the PM space model, a rock is represented by an assemblage of classical elastic units (CU) and nonclassical elastic units

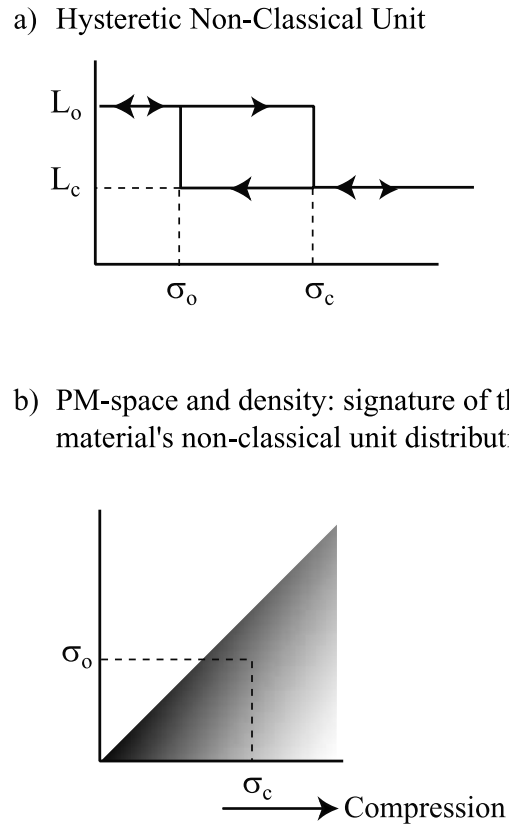


**Figure 13.** (a) Representation of a hysteretic nonclassical unit, and (b) typical example of a PM space density.

(NCU) that behave either reversibly or hysteretically as function of the externally applied stress $\sigma$. The CUs represent the elasticity of the individual grains, whereas the NCUs refer to the elastically soft portions of the material, i.e., the compliant bonding structure. A hysteretic nonclassical unit, H-NCU, can be in only one of two states, open or closed. The behavior of a single H-NCU is such that it is originally open with a length $L_0$, then closes to a length $L_c$ as the applied compression increases to $\sigma_c$ and remains closed as the compression continues to increase. When the applied compression is decreased, the element opens at $\sigma_0$ (different from $\sigma_c$), changing back to its original length $L_0$, and remaining there as compression decreases further (Figure 13a). A large number of such elements with differing $L_0$, $\sigma_0$, $L_c$, and $\sigma_c$ models the heterogeneous elastic elements of the rock's bond system. A reversible nonclassical unit (R-NCU) is an elastic element similar to an H-NCU with identical closing and opening pressures.

[34] The stresses $\sigma_0$ and $\sigma_c$ for each nonclassical element can be used as the element's coordinates in "PM space," thus creating a density of elements in the $\sigma_0-\sigma_c$ space (with $\sigma_0 \leq \sigma_c$). An academic example is shown in Figure 13b (In the gray scale, darker shading corresponds to an increasing density of H-NCU). Reversible elements (R-NCU) reside on the diagonal of the $\sigma_0-\sigma_c$ space. Hysteretic elements (H-NCU) fill the space $\sigma_0 < \sigma_c$. In addition to the PM space, each classical unit (CU) can be represented by a reversible and continuous elastic modulus-stress (EMS)

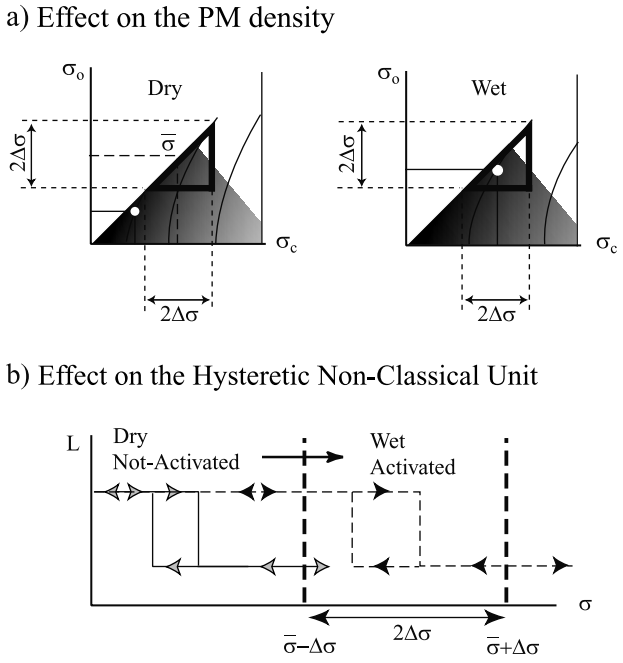


**Figure 14.** Influence of fluid loading on the PM space density and on the behavior of a hysteretic nonclassical unit. The ''activation triangle'' for dynamic experiments is bounded by the diagonal $\sigma_o = \sigma_c$ and the lines $\sigma_o = \bar{\sigma} - \Delta\sigma$ and $\sigma_c = \bar{\sigma} + \Delta\sigma$ (area rimmed by the heavy solid lines).

relation. As the stress on the rock is varied, one can use the PM space representation to keep track of which elements are open and which are closed and to simulate the stress-strain response observed in rock by adding the resulting strain from the NCUs to the elastic strain produced by the CUs calculated from the EMS relation.

[35] In a dynamic experiment, (e.g., sinusoidal cycling between $\bar{\sigma} - \Delta\sigma$ and $\bar{\sigma} + \Delta\sigma$ ($\bar{\sigma}$ being the ambient external stress, and $\Delta\sigma$ the maximum stress excursion), one samples only a small ''activation triangle'' in PM space (Figure 14a) and a small section of the EMS relation. The typical maximum pressure excursions in dynamic measurements are of the order of 0.1 MPa. In terms of the EMS relation and the PM space the dynamic properties of a material can be investigated as follows: the linear dynamic behavior is found by evaluating the local EMS relation at $\bar{\sigma}$; the nonlinear behavior can be probed by studying the density within the ''activation triangle'' in PM space [*Guyer et al.*, 1994, 1995; *McCall and Guyer*, 1994; *Van Den Abeele et al.*, 1997]. In the current model, only the classical units (CU) control the linear modulus of the material. Thus the observed decrease of the stiffness with increasing saturation can be translated to a global decrease of the modulus of each elastic element as function of the level of saturation.

[36] With respect to nonlinear effects, only those nonclassical units which reside inside the PM space ''activation triangle'' will have an impact on to the dynamic response. Elements outside the activation triangle never have a chance to open or close and have therefore not to be considered. A quasi-analytical treatment of PM space reveals that the density of nonclassical elements near the diagonal of the PM space determines the amount of hysteretic nonlinearity: the more NCUs near the diagonal, the larger the nonlinearity. In terms of the observations of moisture influence, the increase of nonlinearity with saturation then simply implies that the density of nonclassical elements within the probed region in PM space increases with saturation. In other words, owing to the net extension of the solid matrix with saturation as a result of an increased fluid loading (decrease of internal contraction or increase of expansion), the same excursion in external stresses in a wet sample will be able to activate more units than for the same sample in a dry state, resulting in a larger density of NCUs in the activation triangle and therefore a higher nonlinearity. The total number of classical elastic elements in PM space is assumed conserved. Only the number (density) of activated nonclassical units increases with saturation. We hypothesize that partial saturation induces a shift in the distribution of (particular populations of) the nonclassical elastic elements in the PM space toward a higher (external) stress range. This is illustrated in Figure 14. We are currently attempting to substantiate and quantify the shift of the NCUs by conducting static stress-strain measurements on partially saturated rock samples and analyzing the corresponding PM spaces at various levels of saturation [*Carmeliet and Van Den Abeele*, 2002].

## 4. Conclusions

[37] The experiments we described in this paper suggest evidence for the role of fluids on the nonlinear behavior of two rock types: pelletoidal limestone (Lavoux) and clay-rich sandstones (Meule and Berea). We conducted dynamic resonance measurements at ambient pressure conditions and at increasing confining pressure. In the pressure vessel experiments we measured Young's mode resonance as a function of confining pressure on saturated and dry samples. In the dynamic measurements at ambient pressure conditions we applied Young's mode resonance on samples as a function of saturation from ~0.1% to 99% saturation. Both linear and nonlinear responses are extremely sensitive to the water saturation, especially at low saturation (<10–20%).

[38] From a macroscopic perspective, at low water saturation the microscopic fluid-solid interactions result in a prestressing of the solid. As saturation increases, the microscopic contraction forces decrease, leading to an expansion of the solid matrix. Owing to this expansion, the dynamic mobility of the material's microscopic and mesoscopic entities increases with saturation, and a reduction of the stiffness together with an increase in damping of the material can be expected. At the same time the number of active nonlinear and/or hysteretic microinhomogeneities (grain-to-grain boundaries, asperities, microcracks, etc.) and their ability to change states (contact–no-contact; open-close; pin-unpin) increases with the degree of saturation. Therefore an increase of nonlinear elastic effects is expected at low saturation (<10–20%). At larger saturation levels (>20%) the effect of the microstresses levels off. In clay-rich materials the capillary pressure can be countered by an extreme swelling pressure, and the nonlinearity may decrease as a result of locking due to high tensile microstresses that are induced.

[39] In terms of modeling implications, we showed that the moisture-induced effects on the nonlinearity in rock can be interpreted as a relocation of nonclassical units in the PM space, which represents the (linear and nonlinear) elastic behavior of the rock's bond system. The increase of nonlinearity points toward an increase of the number of hysteretic elements near the PM space diagonal. This interpretation suggests that moisture is merely an activator of nonlinearity, rather than being the mechanism itself.

[40] **Acknowledgments.** This work was performed under the auspices of the Flemish Institute for the Advancement of Science and Technology in Industry, the Flemish Fund for Scientific Research, the Research Council of the Catholic University of Leuven, Belgium, and the Office of Basic Energy Research, Engineering and Geoscience (contract W-7405-ENG-36), U.S. Department of Energy with the University of California. The authors also acknowledge support by a University Collaborative Research Program of The Institute of Geophysics and Planetary Physics at Los Alamos National Laboratory, New Mexico. Work was also supported in part by the Institut Français du Pétrole, Rueil-Malmaison, France. We are indebted to R. A. Guyer for valuable suggestions and to M. Masson for experimental assistance.

## References

Bazant, Z. P., Constitutive equation for concrete creep and shrinkage based on thermodynamics of multi-phase systems, *Mater. Struct.*, *3*, 3–36, 1970.

Bazant, Z. P., A. B. Hauggaard, S. Baweja, and F.-J. Ulm, Microprestress solidification theory for concrete creep, 1, Aging and drying effects, *J. Eng. Mech.*, *123*, 1188–1194, 1997.

Bear, J., and Y. Bachmat, *Introduction to Modeling of Transport Phenomena in Porous Media*, Kluwer Acad., Norwell, Mass., 1991.

Beresnev, I. A., and K.-L. Wen, Nonlinear soil response—A reality?, *Bull. Seismol. Soc. Am.*, *86*, 1964–1978, 1996.

Binggeli, M., and C. M. Mate, Influence of water vapor on nanotribology studied by friction force microscopy, *J. Vac. Sci. Technol.*, *B13*, 1312–1315, 1995.

Bourbié, T., O. Coussy, and B. Zinszner, *Acoustique des Milieux Poreux*, Technip, Paris, 1986.

Capella, B., and G. Dietler, Force-distance curves by atomic force microscopy, *Surf. Sci.*, *34*, 1–104, 1999.

Carmeliet, J., and K. E.-A. Van Den Abeele, Application of the Preisach-Mayergoyz space model to analyze moisture effects on the nonlinear elastic response of rock, *Geophys. Res. Lett.*, *29*(7), 10.1029/2001GL014243, 2002.

Carmeliet, J., G. Houvenaghel, and F. Descamps, Multiscale network for simulating liquid water and water vapour transfer properties of porous materials, *Transp. Porous Media*, *35*, 67–88, 1999.

Dreyer, W., *The Science of Rock Mechanics*, vol. 1, *The Strength Properties of Rocks*, Trans Tech, Clausthal-Zellerfeld, Germany, 1972.

Durner, W., Hydraulic conductivity estimations for soils with heterogeneous pore structure, *Water Resour. Res.*, *30*, 211–223, 1994.

Field, E. H., P. A. Johnson, I. Beresnev, and Y. Zeng, Nonlinear ground-motion amplification by sediments during the 1994 Northridge earthquake, *Nature*, *390*, 599–602, 1997.

Guyer, R. A., and P. A. Johnson, Nonlinear mesoscopic elasticity: Evidence of a new class of materials, *Phys. Today*, *52*, 30–35, 1999.

Guyer, R. A., K. R. McCall, and G. N. Boitnott, Hysteresis, discrete memory and nonlinear wave propagation in rock, *Phys. Rev. Lett.*, *74*, 3491–3494, 1994.

Guyer, R. A., K. R. McCall, P. A. Johnson, P. N. J. Rasolofosaon, and B. Zinszner, Equation of state hysteresis and resonant bar measurements on rock, in *Proceedings of International Symposium on Rock Mechanics*, edited by J. J. K. Daemon and R. A. Schultz, pp. 177–181, A. A. Balkema, Brookfield, Vt., 1995.

Guyer, R. A., K. R. McCall, G. N. Boitnott, L. B. Hilbert Jr., and T. J. Plona, Quantitative implementation of Preisach-Mayergoyz space to find static and dynamic elastic moduli in rock, *J. Geophys. Res.*, *102*, 5281–5293, 1997.

Hamilton, M. F., Fundamentals and applications of nonlinear acoustics, in *Nonlinear Wave Propagation in Mechanics, Rep. AMD-77*, Am. Soc. of Mech. Eng., New York, 1986.

Hardin, B. O., and V. P. Drnevich, Shear modulus and damping in soils: Measurement and parameter effects, *J. Soil Mech. Found. Div. Am. Soc. Civ. Eng.*, *98*, 603–624, 1972a.

Hardin, B. O., and V. P. Drnevich, Shear modulus and damping in soils: Design equations and curves, *J. Soil Mech. Found. Div. Am. Soc. Civ. Eng.*, *98*, 667–692, 1972b.

Hiller, K. H., Strength reduction and length changes in porous glass caused by water vapour adsorption, *J. Appl. Phys.*, *35*(5), 1622–1628, 1964.

Isihara, K., *Soil Behavior in Earthquake Geotechnics*, Clarendon, Oxford, England, 1996.

Israelachvili, J. N., *Intermolecular and Surface Forces with Application to Colloidal and Biological Systems*, Academic, San Diego, Calif, 1985.

Johnson, P. A., and P. N. J. Rasolofosaon, Manifestation of nonlinear elasticity in rock: Convincing evidence over large frequency and strain intervals from laboratory studies, *Nonlinear Processes Geophys.*, *3*, 77–88, 1996.

Johnson, P. A., B. Zinszner, and P. N. J. Rasolofosaon, Resonance and nonlinear elastic phenomena in rock, *J. Geophys. Res.*, *101*, 11,553–11,564, 1996.

Lucet, N., P. N. J. Rasolofosaon, and B. Zinszner, Sonic properties of rock under confining pressure using the resonant bar technique, *J. Acoust. Soc. Am.*, *89*, 980–990, 1991.

McCall, K. R., and R. A. Guyer, Equation of state and wave propagation in hysteretic nonlinear elastic material, *J. Geophys. Res.*, *99*, 23,887–23,897, 1994.

Naugolnykh, K., and L. Ostrovsky, *Nonlinear Wave Processes in Acoustics*, Cambridge Univ. Press, New York, 1998.

Orr, C., Jr., Application of mercury penetration to materials analysis, *Powder Technol.*, *3*, 117–123, 1969.

Powers, T. C., Mechanism of shrinkage and reversible creep of hardened cement paste, paper presented at International Conference on the Structure of Concrete, Cement and Concr. Assoc., London, U.K, 1965.

Stoker, J. J., *Nonlinear Vibrations in Mecahnical and Electrical Systems*, Wiley-Interscience, New York, 1950.

TenCate, J., and T. J. Shankland, Slow dynamics and nonlinear response at low strains in Berea sandstone, in *Proceedings of the 16th International Congress on Acoustics*, vol. 3, edited by P. Kuhl and L. Crum, pp. 1563–1566, Acoust. Soc. of Am., Seattle, Wash., 1998.

Van Brakel, J., S. Modry, and M. Svata, Mercury porosimetry: State of the art, *Powder Technol.*, *29*, 1–12, 1981.

Van Den Abeele, K. E.-A., P. A. Johnson, R. A. Guyer, and K. R. McCall, On the analytical solution of hysteretic nonlinear response in elastic wave propagation, *J. Acoust. Soc. Am.*, *101*, 1885–1898, 1997.

Van Den Abeele, K. E.-A., P. A. Johnson, and A. Sutin, Nonlinear elastic wave spectroscopy (NEWS) techniques to discern material damage, I, Nonlinear wave modulation spectroscopy (NWMS), *Res. Nondestr. Eval.*, *12*, 17–30, 2000a.

Van Den Abeele, K. E.-A., J. Carmeliet, J. A. TenCate, and P. A. Johnson, Nonlinear elastic wave spectroscopy (NEWS) techniques to discern material damage, II, Single mode nonlinear resonant acoustic spectroscopy (SIMONRAS), *Res. Nondestr. Eval.*, *12*, 31–42, 2000b.

van Genuchten, M. T., A closed-form equation for predicting the hydraulic conductivity of unsaturated soils, *Soil Sci. Soc. Am. J.*, *44*, 892–898, 1980.

Wittmann, F. H., *Bestimmung physikalischer Eigenschaften des Zementsteins, Dtsch. Ausschuss Stahlbeton 232*, pp. 1–63, W. Ernst, Berlin, 1974.

Zinszner, B., P. A. Johnson, and P. N. J. Rasolofosaon, Influence of change in physical state on elastic nonlinear response in rock: Significance of effective pressure and water saturation, *J. Geophys. Res.*, *102*, 8105–8120, 1997.

K. E.-A. Van Den Abeele, Interdisciplinary Research Center, Faculty of Science, Catholic University Leuven Campus Kortrijk, E. Sabbelaan 53, B-8500, Kortrijk, Belgium. (Koen.vandenabeele@kulak.ac.be)

J. Carmeliet, Laboratory of Building Physics, Department of Civil Engineering, Catholic University Leuven, Kasteelpark Arenberg 51, B-3001 Leuven, Belgium. (Jan.Carmeliet@bwk.kuleuven.ac.be)

P. A. Johnson, Earth and Environmental Sciences Division, Geophysics EES-11, MS D443, Los Alamos National Laboratory, Los Alamos, NM 87545, USA. (paj@lanl.gov)

B. Zinszner, Institut Français du Pétrole, B. P. 311-92506, Rueil-Malmaison Cedex, France. (Bernard.Zinszner@ifp.fr)